A New Class of Functionalized Polyoxometalates: Synthetic, Structural, Spectroscopic, and Electrochemical Studies of Organoimido Derivatives of $[Mo_6O_{19}]^{2-}$

Joseph B. Strong,[†] Glenn P. A. Yap,[‡] Robert Ostrander,[‡] Louise M. Liable-Sands,[‡] Arnold L. Rheingold,[‡] René Thouvenot,[§] Pierre Gouzerh,[§] and Eric A. Maatta*[,†]

Contribution from the Department of Chemistry, Kansas State University, Manhattan, Kansas 66506, Department of Chemistry, University of Delaware, Newark, Delaware 19716, and the Laboratoire de Chimie Inorganique et Matériaux Moléculaires, Unité C.N.R.S. 7071, Université Pierre et Marie Curie, 75252 Paris Cedex 05, France

Received August 5, 1999. Revised Manuscript Received November 22, 1999

Abstract: A convenient method for the systematic introduction of a variety of organoimido ligands at terminal oxo sites in the hexamolybdate cluster $[Bu_4N]_2[Mo_6O_{19}]$ is described, consisting of reaction with the appropriate organic isocyanate RNCO (R = *n*-butyl, cyclohexyl, 2,6-diisopropylphenyl) in pyridine solution. Singly functionalized imido-hexamolybdates $[Mo_6O_{18}(NR)]^{2-}$ incorporating each of the above substituents are described. In the case of the 2,6-(diisopropyl)phenylimido ligand (NAr), multiple functionalization has also been achieved: hexamolybdate derivatives $[Mo_6O_{(19-x)}(NAr)_x]^{2-}$ incorporating two, three, four, and five NAr ligands at terminal sites have been prepared. The complexes have been characterized by cyclic voltammetry, multinuclear (^{1}H, ^{14}N, ^{17}O, and ^{95}Mo) NMR and electronic spectroscopy, and single-crystal X-ray diffraction studies.

Introduction

The polyoxometalate ions formed by the early transition metals are a rich and diverse class of inorganic cluster systems characterized by fascinating structural, electrochemical, catalytic, magnetic, medicinal, and photophysical properties.[1] The development of rational methods for the modification and functionalization of polyoxometalate systems may provide the means to exploit more fully these desirable attributes. Preparation of polyoxometalates incorporating various main group, organic, and organometallic fragments now constitutes a significant area of research, whose scope and pace continue to increase.[2]

Among polyoxometalate structures, one of the prototypes is the so-called Lindqvist structure which is adopted by the hexametalates $[M_6O_{19}]^{n-}$ (M = Mo,[3] W,[4] Nb,[5] Ta,[6] and V[7]) as well as by various mixed-metal analogues. The Lindqvist structure is represented below, and consists of a central oxygen

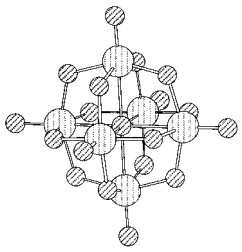

atom about which are arrayed six metal atoms in an octahedral geometry. Each metal bears one terminal oxygen atom, and shares an additional four μ_2-oxygen atoms with adjacent metal atoms. In general, the overall symmetry of these Lindqvist ions approaches O_h.

In the case of the hexamolybdate ion, $[Mo_6O_{19}]^{2-}$,[8] a sizable class of derivatives $[Mo_6O_{18}(L)]^{n-}$ has been prepared in which an exogenous ligand L replaces a terminal oxo ligand within the parent structure. Structurally characterized examples of such

[†] Kansas State University.
[‡] University of Delaware.
[§] Université Pierre et Marie Curie.

(1) (a) An extensive and authoritative treatise on polyoxometalate chemistry is: Pope, M. T. *Heteropoly and Isopoly Oxometalates*; Springer-Verlag: New York, 1983. (b) An updated overview of the field is: Pope, M. T.; Müller, A. *Angew. Chem., Int. Ed. Engl.* **1991**, *30*, 34. (c) A recent monograph highlighting many aspects of current polyoxometalate research is: *Polyoxometalates: From Platonic Solids to Anti-Retroviral Activity*; Pope, M. T., Müller, A., Eds.; Kluwer Academic Publishers: Dordrecht, The Netherlands, 1994. (d) Comprehensive coverage of a broad range of topics within polyoxometalate chemistry can be found in: *Chem. Rev.* **1998**, *98*, 8 (Hill, C. L., guest editor).

(2) Gouzerh, P.; Proust, A. *Chem. Rev.* **1998**, *98*, 77.

(3) X-ray structural studies of $[Mo_6O_{19}]^{2-}$ with various countercations include: (a) Allcock, H. R.; Bissell, E. C.; Shaw, E. T. *Inorg. Chem.* **1973**, *12*, 2963. (b) Garner, C. D.; Howlander, N. C.; Mabbs, F. E.; McPhail, A. T.; Miller, R. W.; Onan, K. D. *J. Chem. Soc., Dalton Trans.* **1978**, 1582. (c) Nagano, O.; Sasaki, Y. *Acta Crystallogr.* **1979**, *B35*, 2387. (d) Clegg, W.; Sheldrick, G. M.; Garner, C. D.; Walton, I. B. *Acta Crystallogr.* **1982**, *B38*, 2906. (e) Dahlstrom, P.; Zubieta, J.; Neaves, B.; Dilworth, J. R. *Cryst. Struct. Commun.* **1982**, *11*, 463. (f) Arzoumanian, H.; Baldy, A.; Lai, R.; Odreman, A.; Metzger, J.; Pierrot, M. *J. Organomet. Chem.* **1985**, *295*, 343. (g) Shoemaker, C. B.; McAfee, L. V.; Shoemaker, D. P.; DeKock, C. W. *Acta Crystallogr.* **1986**, *C42*, 1310. (h) Riera, V.; Ruiz, M. A.; Villafane, F.; Jeannin, Y.; Bois, C. *J. Organomet. Chem.* **1988**, *345*, C4. (i) Zhang, C.; Ozawa, Y.; Hayashi, Y.; Isobe, K. *J. Organomet. Chem.* **1989**, *373*, C21. (j) Bernstein, S. N.; Dunbar, K. R. *Angew. Chem., Int. Ed. Engl.* **1992**, *31*, 1360.

(4) Fuchs, J.; Freiwald, W.; Hartl, H. *Acta Crystallogr.* **1978**, *B34*, 1764.

(5) (a) Lindqvist, I. *Ark. Kemi* **1952**, *5*, 247. (b) Goiffon, A.; Philippot, E.; Maurin, M. *Rev. Chim. Miner.* **1980**, *17*, 466.

(6) Lindqvist, I.; Aronsson, B. *Ark. Kemi* **1954**, *7*, 49.

(7) Although $[V_6O_{19}]^{8-}$ is unknown, the hexavanadate core is present in several structurally characterized systems such as the Rh and Ir derivatives $[(\eta^5\text{-}C_5Me_5)M]_4[V_6O_{19}]$: (a) Hayashi, Y.; Ozawa, Y.; Isobe, K. *Chem. Lett.* **1989**, 425. (b) Chae, H. K.; Klemperer, W. G.; Day, V. W. *Inorg. Chem.* **1989**, *28*, 1423. (c) Hayashi, Y.; Ozawa, Y.; Isobe, K. *Inorg. Chem.* **1991**, *30*, 1025.

10.1021/ja9927974 CCC: $19.00
Published on Web 01/15/2000

systems include the nitrosyl $[Mo_6O_{18}(NO)]^{3-}$,[9] diazenido species $[Mo_6O_{18}(NNAr)]^{3-}$,[10] a hydrazido derivative $[Mo_6O_{18}(NNMePh)]^{2-}$,[11] the organometallic $[Mo_6O_{18}(\eta^5\text{-}C_5Me_5)]^{-}$,[12] and the diazoalkane complex $[Mo_6O_{18}(NNC(Me)Ar)]^{2-}$.[13] The largest class of $[Mo_6O_{18}(L)]^{n-}$ species is the organoimido hexamolybdates $[Mo_6O_{18}(NR)]^{2-}$.[14−21] Organoimido hexamolybdates also include several examples of multiply functionalized systems $[Mo_6O_{(19-x)}(NR)_x]^{2-}$;[16−18,21] presently, these organoimido species are the only class of polyfunctionalized hexamolybdate derivatives.

Here we present an account of our synthesis and characterization of a large class of organoimido-hexamolybdate derivatives, comprising both singly- and multiply-functionalized systems. Results from X-ray crystallography, electronic and multinuclear NMR spectroscopy, and cyclic voltammetry studies are combined to provide a detailed description of this new class of functionalized polyoxometalates. A portion of this work has been communicated previously.[16]

Results

Synthesis. The reactions of $[Bu_4N]_2[Mo_6O_{19}]$ with 1 equiv of various isocyanates RNCO in pyridine occur to afford monosubstituted imido hexamolybdates $[Bu_4N]_2[Mo_6O_{18}(NR)]$ (**1**) in good yield as shown here:

$$[Bu_4N]_2[Mo_6O_{19}] + RNCO \xrightarrow{py} \underset{\mathbf{1}}{[Bu_4N]_2[Mo_6O_{18}(NR)]} + CO_2 \quad (1)$$

1-Bu (R = *n*-butyl)
1-Cy (R = cyclohexyl)
1-Ar (R = 2,6-(*i*-pr)$_2$C$_6$H$_3$)

In the case of **1-Ar**, the reaction was heated at 110 °C for 48 h, while the preparations of **1-Bu** and **1-Cy** were carried out at room temperature for 7 and 3 d, respectively. After the crude reaction products were washed with diethyl ether, crystals of complexes **1** were obtained by room temperature diffusion of diethyl ether vapor into concentrated acetonitrile solutions. **1-Bu** (56% isolated crystalline yield) and **1-Cy** (73%) are golden-brown, while **1-Ar** (50%) is orange-red.

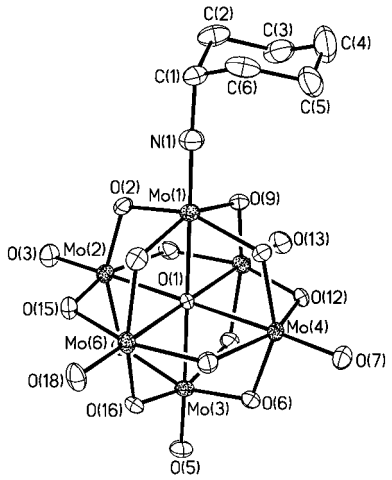

Figure 1. ORTEP diagram of one of the two crystallographically independent $[Mo_6O_{18}(NCy)]^{2-}$ anions of **1-Cy**. Selected bond lengths (Å) and angles (deg) within both anions: Mo(1)−N(1) 1.719(10), 1.711-(14); Mo(2)−O(3) 1.691(8), 1.672(12); Mo(3)−O(5) 1.689(8), 1.668-(9); Mo(4)−O(7) 1.686(8), 1.676(10); Mo(5)−O(13) 1.675(7), 1.676(9); Mo(6)−O(18) 1.689(6), 1.674(10); Mo(1)−O(1) 2.231(6), 2.248(7); Mo(2)−O(1) 2.334(6), 2.322(8); Mo(3)−O(1) 2.334(6), 2.338(7); Mo-(4)−O(1) 2.332(6), 2.325(8); Mo(5)−O(1) 2.341(5), 2.319(7); Mo(6)−O(1) 2.317(5), 2.322(7); Mo(1)−N(1)−C(1) 177.7(7), 176.1(15).

Multiple incorporations of the 2,6-diisopropylphenylimido (NAr) ligand have been accomplished:

$$[Bu_4N]_2[Mo_6O_{19}] + x\text{ArNCO} \xrightarrow[\Delta]{py} [Bu_4N]_2[Mo_6O_{(19-x)}(NAr)_x] + xCO_2 \quad (2)$$

2-Ar ($x = 2$); **3-Ar** ($x = 3$); **4-Ar** ($x = 4$); **5-Ar** ($x = 5$)

Prolonged reaction times (8−12 d) in refluxing pyridine were employed to maximize the isolated yields of these derivatives, and while the crude products generally contain an admixture of higher- and lower-substituted hexamolybdates, in most cases the targeted complexes could be obtained in >90% purity (as judged by cyclic voltammetry and multinuclear NMR spectroscopy) after an initial recrystallization. Using stoichiometric ratios of reactants, crystals of **2-Ar** and **4-Ar** were obtained in yields of 67% and 35%, respectively, after workup as described above. After investigating several variations in reaction conditions and reagent stoichiometries, it was found that excellent yields of **5-Ar** (86%) could be obtained by using a 9:1 ratio of ArNCO/$[Mo_6O_{19}]^{2-}$ in refluxing pyridine for 11 d. Production of **5-Ar** in such high yield under these conditions reflects the increasingly crowded coordination environment within these highly substituted species and the accompanying restrictive orientational requirements for further derivatization: indeed, the synthesis of the hexakis(arylimido) hexamolybdate system $[Mo_6(NAr)_6O_{13}H]^{-}$ requires even more forcing conditions.[21] Within this group of poly-imido hexamolybdates, the isolation of the tris-(NAr) derivative $[Mo_6O_{16}(NAr)_3]^{2-}$, **3-Ar**, has proven to be the most mercurial. Although we have used a variety of reaction times and temperatures in which the ratios of ArNCO/$[Mo_6O_{19}]^{2-}$ have ranged from 2:1 to 18:1, our isolated yields of **3-Ar** have never exceeded 20%.

X-ray Structural Studies. (a) Mono-imido Hexamolybdates. A summary of X-ray crystal data for these systems is provided in Table 1. ORTEP representations of the anions within **1-Cy**, **1-Bu**, and **1-Ar** are presented in Figures 1, 2, and 3,

(8) Synthetic routes to $[Bu_4N]_2[Mo_6O_{19}]$: (a) Fuchs, J.; Jahr, K. F. *Z. Naturforch. B* **1968**, 1380. (b) Che, M.; Fournier, M.; Launay, J. P. *J. Chem. Phys.* **1979**, *71*, 1954. (c) Hur, N. H.; Klemperer, W. G.; Wang, R.-C. *Inorg. Synth.* **1990**, *27*, 77.

(9) (a) Gouzerh, P.; Jeannin, Y.; Proust, A.; Robert, F. *Angew. Chem., Int. Ed. Engl.* **1989**, *28*, 1363. (b) Proust, A.; Thouvenot, R.; Robert, F.; Gouzerh, P. *Inorg. Chem.* **1993**, *32*, 5299.

(10) (a) Hsieh, T.-C.; Zubieta, J. A. *Polyhedron* **1986**, *5*, 1655. (b) Bank, S.; Liu, S.; Shaikh, S. N.; Sun, X.; Zubieta, J.; Ellis, P. D. *Inorg. Chem.* **1988**, *27*, 3535.

(11) Kang, H.; Zubieta, J. *J. Chem. Soc., Chem. Commun.* **1988**, 1192.

(12) (a) Bottomley, F.; Chen, J. *Organometallics* **1992**, *11*, 3404. (b) Proust, A.; Thouvenot, R.; Herson, P. *J. Chem. Soc., Dalton Trans.* **1999**, 51.

(13) Kwen, H.; Young, V. G., Jr.; Maatta, E. A. *Angew. Chem., Int. Ed. Engl.* **1999**, *38*, 1145.

(14) Du, Y.; Rheingold, A. L.; Maatta, E. A. *J. Am. Chem. Soc.* **1992**, *114*, 345.

(15) Errington, R. J.; Lax, C.; Richards, D. G.; Clegg, W.; Fraser, K. A. In ref 1c, p 105.

(16) Strong, J. B.; Ostrander, R.; Rheingold, A. L.; Maatta, E. A. *J. Am. Chem. Soc.* **1994**, *116*, 3601.

(17) Proust, A.; Thouvenot, R.; Chaussade, M.; Robert, F.; Gouzerh, P. *Inorg. Chim. Acta* **1994**, *224*, 81.

(18) Clegg, W.; Errington, R. J.; Fraser, K.; Holmes, S. A.; Schäfer, A. *J. Chem. Soc., Chem. Commun.* **1995**, 455.

(19) Stark, J. L.; Rheingold, A. L.; Maatta, E. A. *J. Chem. Soc., Chem. Commun.* **1995**, 1165.

(20) Stark, J. L.; Young, V. G., Jr.; Maatta, E. A. *Angew. Chem., Int. Ed. Engl.* **1995**, *34*, 2547.

(21) Strong, J. B.; Haggerty, B. S.; Rheingold, A. L.; Maatta, E. A. *J. Chem. Soc., Chem. Commun.* **1997**, 1137.

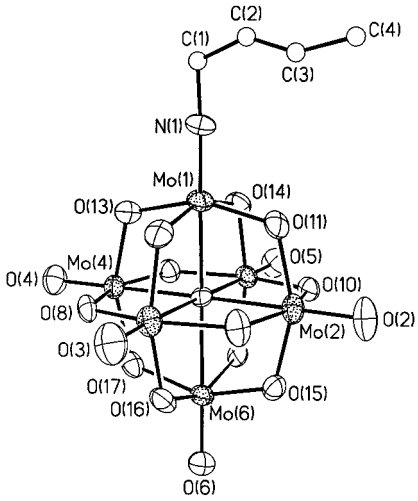

Figure 2. ORTEP diagram of the $[Mo_6O_{18}(NBu)]^{2-}$ anion within **1-Bu**; carbon atoms of the butyl group are drawn as spheres for clarity. Selected bond lengths (Å) and angles (deg): Mo(1)−N(1) 1.720(16); Mo(2)−O(2) 1.722(14); Mo(3)−O(3) 1.646(14); Mo(4)−O(4) 1.671-(13); Mo(5)−O(5) 1.666(13); Mo(6)−O(6) 1.682(12); Mo(1)−O(1) 2.239(10); Mo(2)−O(1) 2.313(11); Mo(3)−O(1) 2.328(11); Mo(4)−O(1) 2.346(11); Mo(5)−O(1) 2.335(11); Mo(6)−O(1) 2.348(10); Mo-(1)−N(1)−C(1) 175.4(17).

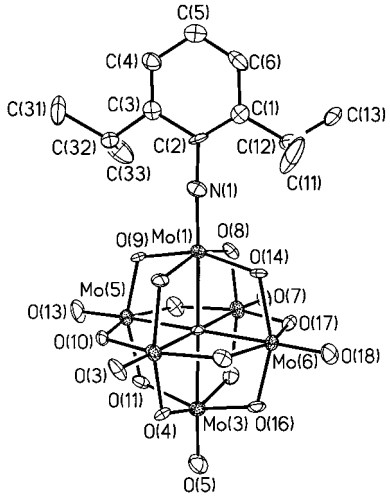

Figure 3. ORTEP diagram of the $[Mo_6O_{18}(NAr)]^{2-}$ anion within **1-Ar**. Selected bond lengths (Å) and angles (deg): Mo(1)−N(1) 1.739(15); Mo(2)−O(3) 1.698(13); Mo(3)−O(5) 1.649(14); Mo(4)−O(7) 1.655-(12); Mo(5)−O(13) 1.668(13); Mo(6)−O(18) 1.711(12); Mo(1)−O(1) 2.254(10); Mo(2)−O(1) 2.337(12); Mo(3)−O(1) 2.312(10); Mo(4)−O(1) 2.322(12); Mo(5)−O(1) 2.344(10); Mo(6)−O(1) 2.320(10); Mo-(1)−N(1)−C(2) 176.3(15).

respectively, along with selected bond lengths and angles; in the case of **1-Cy**, there are two crystallographically independent anions within its asymmetric unit. In each of these mono-imido hexamolybdates, the organoimido ligand occupies a terminal site on the hexamolybdate cage. The short Mo−N bond lengths (**1-Cy**: 1.719(10), 1.711(14) Å; **1-Bu**: 1.720(16) Å; **1-Ar**: 1.739(15) Å) and near-linear Mo−N−C bond angles (**1-Cy**: 177.7(7), 176.1(15)°; **1-Bu**: 175.4(17)°; **1-Ar**: 176.3(15)°) are typical of organoimido ligands bound at an octahedral d^0 metal center and are consistent with a substantial degree of Mo≡N triple bond character.[22] While there are no substantial variations observed in the terminal Mo≡O bond lengths within any of the three structures, in each complex the bond length from the imido-bearing Mo(1) atom to the central O_c atom is significantly shorter than the corresponding Mo−O_c distance involving the trans [O≡Mo] site. The magnitudes of these discrepancies are as follows: **1-Bu**, 0.11 Å; **1-Cy**, 0.10, 0.09 Å; and **1-Ar**, 0.06 Å. Similar displacements of the O_c atom toward the substituted metal site have been observed in the structures of other $[Mo_6O_{18}(L)]^{n-}$ derivatives[9−17,19,20] as well as in those of $[(\eta^5\text{-}C_5H_5)Ti(Mo_5O_{18})]^{3-}$ [23] and $[W_6O_{18}(NAr)]^{2-}$.[24]

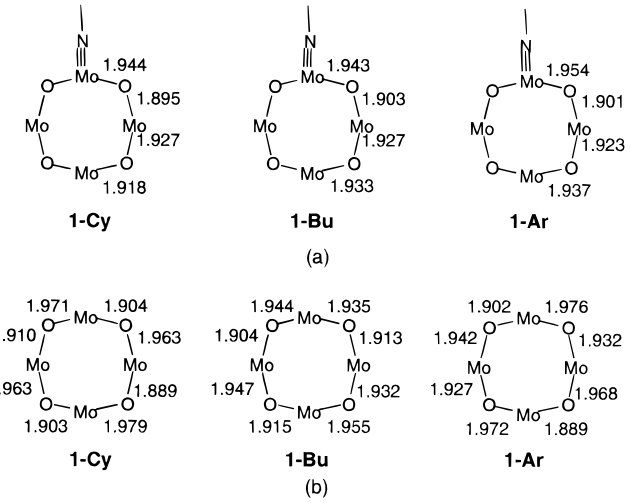

Figure 4. (a) Site-averaged bond lengths (Å) within the longitudinal $\{Mo_4(O_b)_4\}$ belts of **1-Cy** (esd range = 0.006−0.011 Å), **1-Bu** (esd range = 0.011−0.013 Å), and **1-Ar** (esd range = 0.011−0.013 Å). The values for **1-Cy** are averaged for the two independent anions within its asymmetric unit. (b) Bond lengths (Å) within the equatorial $\{Mo_4(O_b)_4\}$ belts of **1-Cy** (esd range = 0.006−0.011 Å), **1-Bu** (esd range = 0.011−0.013 Å), and **1-Ar** (esd range = 0.011−0.013 Å). The values for **1-Cy** are averaged for the two independent anions within its asymmetric unit.

Table 1. Summary of Crystallographic Data for Mono-imido Hexamolybdates

	1-Bu	**1-Cy**	**1-Ar**
formula	$C_{36}H_{81}Mo_6N_3O_{18}$	$C_{38}H_{83}Mo_6N_3O_{18}$	$C_{44}H_{89}Mo_6N_3O_{18}$
formula wt.	1419.7	1445.7	1523.8
cryst system	orthorhombic	triclinic	orthorhombic
space group	*Pbca*	*P*(−1)	*Pbca*
a (Å)	16.873(3)	12.489(3)	18.432(7)
b (Å)	20.048(3)	19.340(5)	20.580(9)
c (Å)	31.706(6)	23.022(6)	31.379(12)
α (deg)		94.08(2)	
β (deg)		103.14(2)	
γ (deg)		91.65(2)	
V (Å^3)	10726(3)	5395.8(25)	11903(8)
Z	8	4	8
D(calc), g cm^{-3}	1.758	1.780	1.701
μ(Mo Kα), cm^{-1}	14.25	14.18	12.91
temp, K	293(2)	245(2)	236(2)
T(max)/*T*(min)	0.190/0.165		
no. of indpt rflns	8406	18960	10467
no of indpt obsvd rflns $F_o \geq 4\sigma(F_o)$	3729	11804	5286
R(*F*), %	6.95[a]	6.19[a]	7.80[a]
R(*wF*), %	7.46[a]	8.55[a]	10.56[a]
N_o/N_v	9.1	14.2	8.3

[a] Quantity minimized = $\sum\Delta^2$; $R = \sum\Delta/\sum(F_o)$; $R(w) = \sum\Delta w^{1/2}/\sum(F_o w^{1/2})$; $\Delta = |(F_o - F_c)|$.

(22) Wigley, D. E. *Prog. Inorg. Chem.* **1994**, *42*, 239.

(23) Che, T. M.; Day, V. W.; Francesconi, L. C.; Fredrich, M. F.; Klemperer, W. G.; Shum, W. *Inorg. Chem.* **1985**, *24*, 4055.

(24) Mohs, T. R.; Yap, G. P. A.; Rheingold, A. L.; Maatta, E. A. *Inorg. Chem.* **1995**, *34*, 9.

Table 2. Summary of Crystal Data for Poly(arylimido) Hexamolybdates

	2-Ar	**3-Ar·3C$_2$H$_4$Cl$_2$**	**4-Ar·2CH$_3$CN**	**5-Ar·2C$_2$H$_4$Cl$_2$**
formula	$C_{56}H_{106}Mo_6N_4O_{17}$	$C_{74}H_{135}Cl_6Mo_6N_5O_{16}$	$C_{84}H_{146}Mo_6N_8O_{15}$	$C_{96}H_{165}Cl_4Mo_6N_7O_{14}$
formula wt.	1683.1	2139.2	2083.7	2358.8
cryst system	triclinic	triclinic	monoclinic	monoclinic
space group	$P(-1)$	$P(-1)$	$P2_1/n$	$C2/c$
a (Å)	12.863(5)	19.573(4)	16.227(9)	59.943(9)
b (Å)	12.829(5)	21.725(5)	22.868(7)	15.487(4)
c (Å)	22.090(12)	23.668(6)	26.766(13)	28.986(6)
α (deg)	88.51(3)	92.03(3)		
β (deg)	86.21(3)	101.77(3)	93.30(4)	112.02(2)
γ (deg)	78.19(3)	98.51(2)		
V (Å^3)	3560(2)	9691(4)	9916(8)	24945.6(8)
Z	2	4	4	8
D(calc), g cm^{-3}	1.570	1.462	1.396	1.256
μ(Mo Kα), cm^{-1}	10.87	9.70	7.95	7.22
temp, K	248(2)	220(2)	233(2)	220(2)
T(max)/T(min)	0.796/0.666		0.654/0.504	
no. of indpt rflns	11207	14127	12955	15319
no. of indpt obsvd rflns $F_o \geq 4\sigma(F_o)$	5511	8920	7353	9210
$R(F)$, %	9.54[a]	9.65[a]	6.51[a]	11.03[b]
$R(wF)$, %	13.25[a]	13.83[a]	8.45[a]	29.68[b,c]
N_o/N_v	11.8	11.7	7.3	10.2

[a] Quantity minimized = $\sum\Delta^2$; $R = \sum\Delta/\sum(F_o)$; $R(w) = \sum\Delta w^{1/2}/\sum(F_o w^{1/2})$; $\Delta = |(F_o - F_c)|$. [b] Quantity minimized = $R(wF^2) = \sum[w(F_o^2 - F_c^2)^2]/\sum[(wF_o^2)^2]^{1/2}$; $R = \sum\Delta/\sum(F_o)$; $\Delta = |(F_o - F_c)|$. [c] $R(wF^2)$, %.

Bond length information for the longitudinal (i.e., those containing the [Mo≡NR] unit) and equatorial [$Mo_4(O_b)_4$] belts within **1-Cy**, **1-Bu**, and **1-Ar** is displayed in Figure 4. Within the longitudinal belts, a slight, but consistent lengthening of the Mo−O_b bonds at the [Mo≡NR] sites can be discerned, and is the expected result of replacing an $[Mo{\equiv}O]^{4+}$ unit with a more electron-rich $[Mo{\equiv}NR]^{4+}$ unit. Similar, albeit more pronounced, effects were first detailed for the [Ti−O_b] sites of [(η^5-C_5H_5)Ti(Mo_5O_{18})]$^{3-}$ as described by Klemperer et al.[23] and were subsequently observed by Bank et al. for the [(C_6F_5NN)-Mo−O_b] sites within [Mo_6O_{18}(NNC_6F_5)]$^{3-}$.[10b] As seen in Figure 4b, the [Mo−O_b] bond lengths within the equatorial rings of the three complexes generally adhere to the pattern of short/long trans bond alternation that was originally noted for [Mo_6O_{19}]$^{2-}$ and [W_6O_{19}]$^{2-}$ by Fuchs,[4] and subsequently described for both [(η^5-C_5H_5)Ti(Mo_5O_{18})]$^{3-}$ [23] and [Mo_6O_{18}-(NNC_6F_5)]$^{3-}$.[10b]

(b) Poly-imido Hexamolybdates. A summary of X-ray crystal data for these systems is provided in Table 2. ORTEP representations of the anions within **2-Ar**, **3-Ar**, **4-Ar**, and **5-Ar** are provided in Figures 5−8, respectively, along with selected bond lengths and angles. For **3-Ar**, only one of the two crystallographically independent anions within its unit cell is shown in Figure 6. In each of these multiply substituted derivatives, the organoimido ligands occupy terminal positions and the metrical parameters associated with the [Mo≡NAr] units are unexceptional. The substitution pattern within these derivatives is noteworthy: contrary to expectations based on steric considerations, the structures of **2-Ar** (cis), **3-Ar** (fac), and **4-Ar** (cis) reveal a preference for mutual cis-coordination of [NAr] ligands, suggesting that the presence of an extant [NAr] group exerts an activating effect at proximal [Mo≡O] sites.

Along the *trans*-[O≡Mo]−O_c−[Mo≡NAr] axes within each of the multiply substituted species, the central O_c oxygen is again displaced away from the [O≡Mo] site toward the *trans*-[Mo≡NAr] site. The magnitudes of this structural *trans*-influence are as follows: for **2-Ar**, 0.21(1) and 0.07(1) Å; for **3-Ar**, 0.17(2), 0.20(2) and 0.16(2) Å (averages of symmetry-related sites within the two independent anions); for **4-Ar**, 0.12(1) and 0.16(1) Å; and for **5-Ar**, 0.12(1) Å.

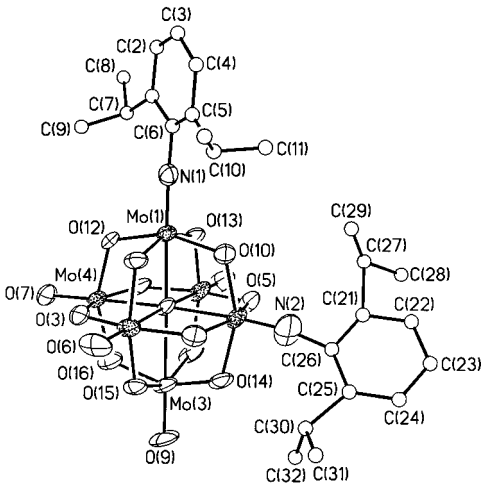

Figure 5. ORTEP diagram of the $[Mo_6O_{17}(NAr)_2]^{2-}$ anion within **2-Ar**. Selected bond lengths (Å) and angles (deg): Mo(1)−N(1) 1.738(14); Mo(2)−N(2) 1.612(26); Mo(3)−O(9) 1.674(14); Mo(4)−O(7) 1.708-(13); Mo(5)−O(8) 1.695(14); Mo(6)−O(6) 1.685(14); Mo(1)−O(1) 2.199(10); Mo(2)−O(1) 2.255(12); Mo(3)−O(1) 2.407(10); Mo(4)−O(1) 2.324(13); Mo(5)−O(1) 2.332(11); Mo(6)−O(1) 2.347(11); Mo-(1)−N(1)−C(6) 175.1(13); Mo(2)−N(2)−C(26) 161.3(24).

Keeping in mind the relatively low precision of the structure determinations, a consistent pattern nonetheless is discernible throughout this series: Mo−O_b bond lengths are generally longer at [Mo≡NAr] sites than at [Mo≡O] sites. An illustration of this trend is provided in Figure 9, which presents the average [Mo−O_b] distances within the [$Mo_4(O_b)_4$] belts of both **2-Ar** and **4-Ar**. This trend is maintained both within the individual [$Mo_4(O_b)_4$] belts of each complex and between the complementary belts of the two complexes (note that the structures of **2-Ar** and **4-Ar** are related by a mutual transposition of their [Mo≡NAr] and [Mo≡O] sites).

Electronic Spectroscopy. Visible region electronic spectral data are collected in Table 3. For the two mono-alkylimido systems, **1-Cy** and **1-Bu**, both the energies (λ_{max} = 325 and 329 nm, respectively) and the molar absorptivities (ϵ = 7000 and 6000 M^{-1} cm^{-1}, respectively) of the lowest energy electronic absorptions are similar to that of the [Mo_6O_{19}]$^{2-}$

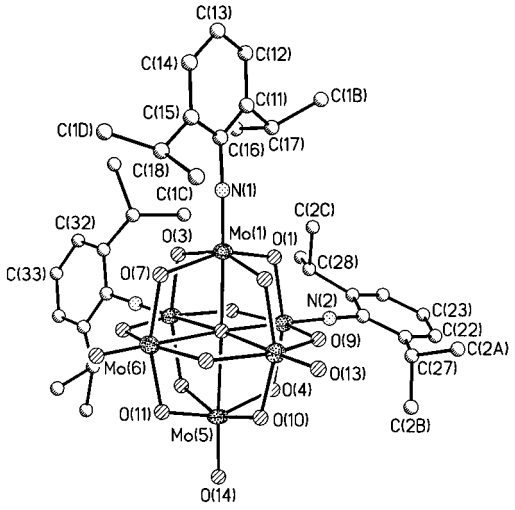

Figure 6. ORTEP diagram of one of the two crystallographically independent $[Mo_6O_{16}(NAr)_3]^{2-}$ anions of **3-Ar**. Selected bond lengths (Å) and angles (deg) within both anions: Mo(1)−N(1) 1.695(26), 1.701(21); Mo(2)−N(2) 1.705(24), 1.710(25); Mo(3)−N(3) 1.745(20), 1.699(24); Mo(4)−O(13) 1.718(18), 1.704(23); Mo(5)−O(14) 1.700(25), 1.676(22); Mo(6)−O(15) 1.641(22), 1.762(20); Mo(1)−O(16) 2.235(21), 2.249(17); Mo(2)−O(16) 2.187(18), 2.225(18); Mo(3)−O(16) 2.212(14), 2.243(17); Mo(4)−O(16) 2.420(14), 2.406(18); Mo(5)−O(16) 2.398(21), 2.375(17); Mo(6)−O(16) 2.433(18), 2.385(17); Mo(1)−N(1)−C(16) 177.3(16), 174.6(18); Mo(2)−N(2)−C(26) 174.0(19), 174.0(17); Mo(3)−N(3)−C(36) 175.1(23), 170.9(20).

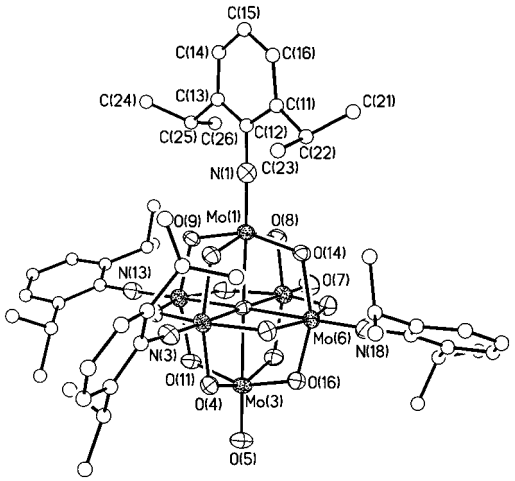

Figure 7. ORTEP diagram of the $[Mo_6O_{15}(NAr)_4]^{2-}$ anion within **4-Ar**; carbon atoms are shown as spheres for clarity. Selected bond lengths (Å) and angles (deg): Mo(1)−N(1) 1.760(10); Mo(2)−N(3) 1.710(10); Mo(5)−N(13) 1.731(11); Mo(6)−N(18) 1.742(11); Mo(3)−O(5) 1.704(8); Mo(4)−O(7) 1.686(9); Mo(5)−O(1) 2.292(8); Mo(6)−O(1) 2.282(8); Mo(1)−N(1)−C(12) 178.8(10); Mo(2)−N(3)−C(32) 177.8(9); Mo(5)−N(13)−C(52) 175.5(10); Mo(6)−N(18)−C(72) 178.5(9).

parent (λ_{max} = 325 nm; ϵ = 6300 M^{-1} cm^{-1}). In contrast, the spectra of the three mono-arylimido hexamolybdates **1-Ph**, **1-Tol**, and **1-Ar** are bathochromically shifted by ca. 25 nm and are considerably more intense. If, as seems reasonable, these charge-transfer transitions originate in a state dominated by Mo−N π-bonding, then the bathochromic shift observed for the mono-arylimido systems can be attributed to a relative destabilization of the particular Mo−N π-bonding level as a result of the mixing in of some $N-C_{ipso}$ π^* character, which is not a factor for the alkylimido systems.[25]

(25) Devore, D. D.; Lichtenhan, J. L.; Takusagawa, F.; Maatta, E. A. *J. Am. Chem. Soc.* **1987**, *109*, 7408.

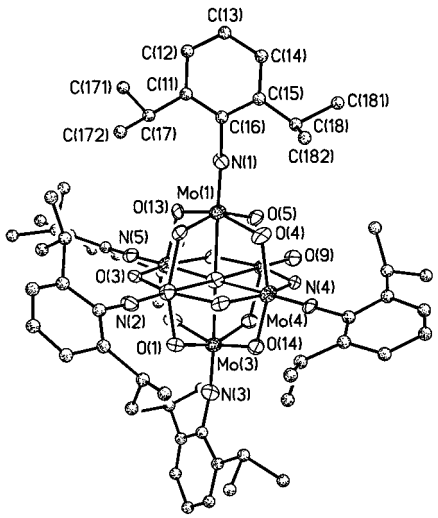

Figure 8. ORTEP diagram of the $[Mo_6O_{14}(NAr)_5]^{2-}$ anion within **5-Ar**; carbon atoms are shown as spheres for clarity. Selected bond lengths (Å) and angles (deg): Mo(1)−N(1) 1.698(14); Mo(2)−N(2) 1.729(14); Mo(3)−N(3) 1.706(14); Mo(4)−N(4) 1.686(14); Mo(5)−N(5) 1.70(2); Mo(6)−O(9) 1.699(12); Mo(1)−O(11) 2.321(12); Mo(2)−O(11) 2.268(11); Mo(3)−O(11) 2.270(12); Mo(4)−O(11) 2.285(12); Mo(5)−O(11) 2.300(12); Mo(6)−O(11) 2.388(11); Mo(1)−N(1)−C(16) 176.4(13); Mo(2)−N(2)−C(26) 173.3(14); Mo(3)−N(3)−C(36) 171.5(13); Mo(4)−N(4)−C(46) 175.4(13); Mo(5)−N(5)−C(56) 173.6(12).

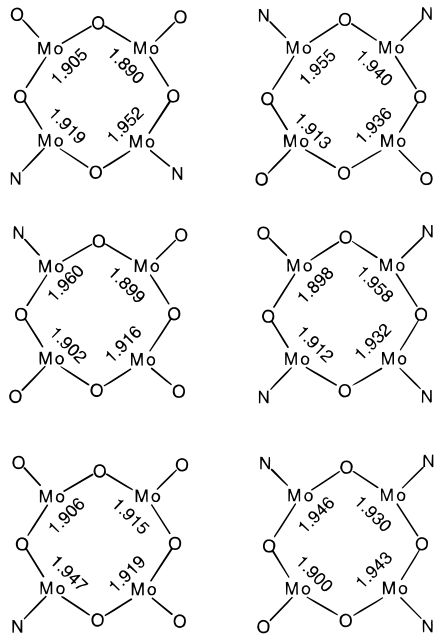

Figure 9. Comparison of average {Mo−O_b} distances (Å) at the [Mo≡NAr] and [Mo≡O] sites within the complementary $\{Mo_4(O_b)_4\}$ belts of **2-Ar** (left) and **4-Ar** (right).

Within the arylimido series $[Mo_6O_{(19-x)}(NAr)_x]^{2-}$, λ_{max} values generally are observed to shift to lower energies with increasing [NAr] incorporation, although the band maxima recorded for **4-Ar** and **5-Ar** are identical. Also evident in Table 3 is the virtual additivity of the ϵ values accompanying incremental [NAr] incorporation.

Cyclic Voltammetry. Table 4 presents $E_{1/2}$ values as determined by cyclic voltammetry for the reductions of the $[Mo_6O_{(19-x)}(NR)_x]^{2-}$ to the corresponding trianions. It is seen that every organoimido hexamolybdate complex is more difficult to reduce than is the $[Mo_6O_{19}]^{2-}$ parent. This observation clearly indicates that organoimido ligands are superior to oxo ligands

Table 3. Visible Region Spectral Data for Complexes $[Mo_6O_{(19-x)}(NR)_x]^{2-}$ [a]

complex	λ_{max}, nm	ϵ, M^{-1} cm^{-1}
$[Mo_6O_{19}]^{2-}$ [b]	325	6300
$[Mo_6O_{18}(NCy)]^{2-}$ (**1-Cy**)	325	7000
$[Mo_6O_{18}(NBu)]^{2-}$ (**1-Bu**)	329	6000
$[Mo_6O_{18}(NPh)]^{2-}$ (**1-Ph**)[b]	342	20000
$[Mo_6O_{18}(NTol)]^{2-}$ (**1-Tol**)[c]	348	23000
$[Mo_6O_{18}(NAr)]^{2-}$ (**1-Ar**)	351	19000
$[Mo_6O_{17}(NAr)_2]^{2-}$ (**2-Ar**)	356	30000
$[Mo_6O_{16}(NAr)_3]^{2-}$ (**3-Ar**)	361	42000
$[Mo_6O_{15}(NAr)_4]^{2-}$ (**4-Ar**)	364	58000
$[Mo_6O_{14}(NAr)_5]^{2-}$ (**5-Ar**)	364	77000

[a] $[Bu_4N]^+$ salts, CH_3CN solution, 298 K. [b] From ref 17. [c] From ref 14.

Table 4. Cyclic Voltammetry Data for Complexes $[Mo_6O_{(19-x)}(NR)_x]^{2-}$ [a]

complex	$E_{1/2}$, mV[b]
$[Mo_6O_{19}]^{2-}$	−707
$[Mo_6O_{18}(NPh)]^{2-}$ (**1-Ph**)[c]	−907
$[Mo_6O_{18}(NBu)]^{2-}$ (**1-Bu**)	−983
$[Mo_6O_{18}(NCy)]^{2-}$ (**1-Cy**)	−994
$[Mo_6O_{18}(NAr)]^{2-}$ (**1-Ar**)	−958
$[Mo_6O_{17}(NAr)_2]^{2-}$ (**2-Ar**)	−1168
$[Mo_6O_{16}(NAr)_3]^{2-}$ (**3-Ar**)	−1392
$[Mo_6O_{15}(NAr)_4]^{2-}$ (**4-Ar**)	−1596
$[Mo_6O_{14}(NAr)_5]^{2-}$ (**5-Ar**)	−2038[d]

[a] $[Bu_4N]^+$ salts, CH_3CN solution, 298 K, Pt working electrode, $[Bu_4N]PF_6$ supporting electrolyte, 100 mV s^{-1}. [b] $E_{1/2}$ vs Ag/Ag^+. [c] From ref 17. [d] E_{pc} (irreversible reduction).

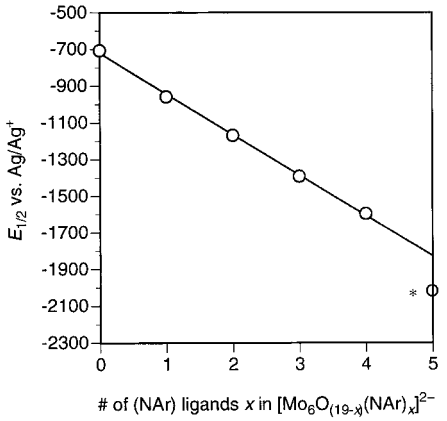

Figure 10. Correlation between the degree of substitution in $[Mo_6O_{(19-x)}(NAr)_x]^{2-}$ complexes and their $E_{1/2}$ values. An asterisk indicates an E_{pc} value for an irreversible reduction.

as electron donors.[26] Within the group of mono-imido hexamolybdates, the reduction potentials (vs Ag/Ag^+) are observed to shift cathodically in the order **1-Ph** (−907 mV) > **1-Ar** (−958 mV) > **1-Bu** (−983 mV) > **1-Cy** (−994 mV); this sequence is in accord with the relative inductive donor effects expected for the substitutents within this group of organoimido ligands.

For the series $[Mo_6O_{(19-x)}(NAr)_x]^{2-}$, a continual accumulation of electron density accompanying progressive [NAr] incorporation is revealed by a steady decrease in $E_{1/2}$ values. This relationship is presented graphically in Figure 10. The addition of each successive [NAr] ligand drives the reduction potential of the $[Mo_6O_{(19-x)}(NAr)_x]^{2-}$ system more negative by ca. 220 mV; the correlation is near-linear for $[Mo_6O_{19}]^{2-}$, **1-Ar**, **2-Ar**, **3-Ar**, and **4-Ar**. In the case of **5-Ar**, the reduction was observed to be irreversible at $E_{pc} = -2038$ mV.

(26) (a) Nugent, W. A.; Mayer, J. M. *Metal−Ligand Multiple Bonds*; Wiley: New York, 1988. (b) Hogarth, G.; Konidaris, P. C.; Saunders, G. C. *J. Organomet. Chem.* **1991**, *406*, 153.

Table 5. ^{95}Mo NMR Data for Complexes $[Mo_6O_{(19-x)}(NR)_x]^{2-}$ [a,b]

complex	$\delta(^{95}Mo{\equiv}NR)$	$\delta(^{95}Mo{\equiv}O)$	$\delta(^{95}Mo)_{wt}$[c]
$[Mo_6O_{19}]^{2-}$		127	
$[Mo_6O_{18}(NCy)]^{2-}$ (**1-Cy**)	1[d]	153	
$[Mo_6O_{18}(NBu)]^{2-}$ (**1-Bu**)	−2[d]	152	
$[Mo_6O_{18}(NPh)]^{2-}$ (**1-Ph**)[e]	68[d]	148	
$[Mo_6O_{18}(NAr)]^{2-}$ (**1-Ar**)	123[d]	152	147
$[Mo_6O_{17}(NAr)_2]^{2-}$ (**2-Ar**)	126[d]	172	157
$[Mo_6O_{16}(NAr)_3]^{2-}$ (**3-Ar**)	130	191	161
$[Mo_6O_{15}(NAr)_4]^{2-}$ (**4-Ar**)	136	209	160
$[Mo_6O_{14}(NAr)_5]^{2-}$ (**5-Ar**)	146	225	159

[a] $[Bu_4N]^+$ salts, CH_3CN solution, 343 K. [b] ^{95}Mo chemical shifts (in ppm) referenced to external Na_2MoO_4 at pH 11. [c] $\delta(^{95}Mo)_{wt} = (1/6)\sum(n\delta(^{95}Mo))$. [d] $^1J_{^{14}N-^{95}Mo} \approx 50$ Hz. [e] From ref 17.

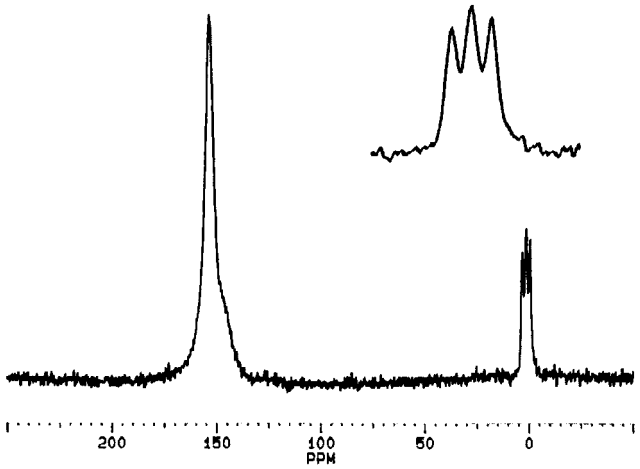

Figure 11. The 26 MHz ^{95}Mo NMR spectrum of **1-Cy** (CH_3CN, 333 K, unlocked, 36 μs (90°) flip angle, 24200 scans without recycle delay, acquisition time 0.102 s/scan); the inset shows the expanded [Mo≡NCy] resonance at $\delta = 1$ as a 1:1:1 triplet due to scalar coupling with ^{14}N ($^1J_{^{14}N-^{95}Mo} \approx 50$ Hz).

^{95}Mo NMR Spectroscopy. Data are summarized in Table 5. For each of the mono-imido complexes $[Mo_6O_{18}(NR)]^{2-}$, the resonance for the imido-bearing $[^{95}Mo{\equiv}NR]$ site could be unambiguously identified because of its appearance as a 1:1:1 triplet due to scalar coupling ($^1J_{^{14}N-^{95}Mo} \approx 50$ Hz). Figure 11 presents the ^{95}Mo NMR spectrum of **1-Cy**. For the two mono-alkylimido complexes **1-Cy** ($\delta = 1$) and **1-Bu** ($\delta = -2$), the $[^{95}Mo{\equiv}NR]$ resonances are considerably shielded with respect to $[Mo_6O_{19}]^{2-}$ ($\delta = 127$). For the mono-arylimido complexes **1-Ph** ($\delta = 68$[17]) and **1-Ar** ($\delta = 123$), this upfield shift is much less pronounced. For these $[Mo_6O_{18}(NR)]^{2-}$ systems, their virtual C_{4v} symmetry generates two $[^{95}Mo{\equiv}O]$ environments, cis and trans to the [Mo≡NR] site, for which two resonances in a 4:1 ratio could be expected. As can be seen in Figure 11, the $[^{95}Mo{\equiv}O]$ resonance of **1-Cy** ($\delta = 153$) displays a barely resolved shoulder of lesser intensity on its upfield side; the $[^{95}Mo{\equiv}O]$ resonances for **1-Bu** ($\delta = 152$) and **1-Ar** ($\delta = 152$) display similar, albeit less conspicuous dissymmetry leading us to suspect that the expected two $[^{95}Mo{\equiv}O]$ resonances are virtually degenerate.

Within the $[Mo_6O_{(19-x)}(NAr)_x]^{2-}$ series, increasing the number of [NAr] ligands induces a slight but steady deshielding progression in $\delta(^{95}Mo{\equiv}NR)$: **1-Ar** ($\delta = 123$), **2-Ar** ($\delta = 126$), **3-Ar** ($\delta = 130$), **4-Ar** ($\delta = 136$), and **5-Ar** ($\delta = 146$). Scalar coupling with $^1J_{^{14}N-^{95}Mo} \approx 50$ Hz was observed in most cases, although it was barely detectable for **4-Ar** and not discernible in the broadened resonance of **5-Ar**; at least in part, this lack of resolution may derive from the presence of two symmetry-distinct $[^{95}Mo{\equiv}NR]$ sites within **4-Ar** (C_{2v}) and **5-Ar** (C_{4v}).

Table 6. ^{14}N NMR Data for $[Mo_6O_{(19-x)}(NR)_x]^{2-}$ Complexes[a,b]

complex	$\delta(^{14}NR)$
$[Mo_6O_{18}(NBu)]^{2-}$ (**1-Bu**)	60.9
$[Mo_6O_{18}(NAr)]^{2-}$ (**1-Ar**)	30.6
$[Mo_6O_{17}(NAr)_2]^{2-}$ (**2-Ar**)	27.7
$[Mo_6O_{16}(NAr)_3]^{2-}$ (**3-Ar**)	24.4
$[Mo_6O_{15}(NAr)_4]^{2-}$ (**4-Ar**)	21.4
$[Mo_6O_{14}(NAr)_5]^{2-}$ (**5-Ar**)	18.3

[a] $[Bu_4N]^+$ salts, CH_3CN solution, 343 K, 36.1 MHz. [b] ^{14}N chemical shifts (ppm) with respect to neat liquid nitromethane.

Progressive [NAr] incorporation within the $[Mo_6O_{(19-x)}(NAr)_x]^{2-}$ series should also produce broadened ^{95}Mo NMR resonances as a result of a longer rotational correlation time τ_c and consequently a shorter spin−spin relaxation time (T_2) as the complexes become larger. At the [^{95}Mo≡O] sites within this series, increasing [NAr] incorporation produces a substantial downfield progression in the ^{95}Mo chemical shifts: **1-Ar** (δ = 152), **2-Ar** (δ = 172), **3-Ar** (δ = 191), **4-Ar** (δ = 209), and **5-Ar** (δ = 225).

Also included in Table 5 is a compilation of the weighted average of the $\delta(^{95}Mo)$ values for the six Mo atoms within each of the $[Mo_6O_{(19-x)}(NAr)_x]^{2-}$ complexes. It can be seen that an essentially constant value of ca. 160 ppm is maintained for **2-Ar**, **3-Ar**, **4-Ar**, and **5-Ar** (despite a growing disparity between the chemical shifts of the [^{95}Mo≡O] sites and the [^{95}Mo≡NR] sites within the series), suggesting that the total electron density of the six Mo atoms has attained a limiting value.

It should be noted that an authentic sample of **3-Ar** was not available for these studies because of the synthetic difficulties associated with its large-scale preparation (vide supra) and therefore the assignment of its spectrum derives from studies of samples containing mixtures of various $[Mo_6O_{(19-x)}(NAr)_x]^{2-}$ species; our proposed assignments for **3-Ar** are, however, based upon our knowledge of the composition of these mixed samples as determined by cyclic voltammetry studies, and are consistent with results obtained in ^{14}N NMR studies.

^{14}N NMR Spectroscopy. ^{14}N chemical shifts for the organoimido ligands within the complexes are collected in Table 6, and the spectra of the $[Mo_6O_{(19-x)}(NAr)_x]^{2-}$ systems are presented in Figure 12. The ^{14}N resonance for **1-Bu** is observed at significantly lower field (60.9 ppm) than the arylimido ligand resonance of **1-Ar** (30.6 ppm). A similar effect has been noted in the ^{14}N NMR spectra of the d^0 tungsten systems [RN≡WCl_4(THF)]: for R = Et, the ^{14}N resonance is observed at 78.3 ppm, considerably downfield of that observed for the case when R = Ph (53.2 ppm).[27] Each successive incorporation of an [NAr] ligand into the hexamolybdate framework induces an upfield shift in $\delta(^{14}NAr)$ of ca. −3 ppm as shown in Figure 13. As noted above, the symmetries of **4-Ar** (C_{2v}) and **5-Ar** (C_{4v}) generate two differentiated [NAr] environments within each of these derivatives for which distinct ^{14}N resonances (in ratios of 2:2 and 4:1, respectively) could be expected, but which were not resolved. Given the relatively narrow dispersion of the $\delta(^{14}N)$ values throughout this series, it is reasonable to conclude that the chemical shifts of these symmetry-distinct [NAr] sites are virtually coincident.

The observation of an *upfield* progression in δ(Mo≡^{14}NAr) accompanying a *downfield* progression in δ(^{95}Mo≡NAr) for the $[Mo_6O_{(19-x)}(NAr)_x]^{2-}$ series is striking and is at variance with previous results from multinuclear NMR studies of various monometallic organoimido systems [L_nM≡NR].[27] Our ^{17}O NMR results (vide infra) also demonstrate this counter-intuitive relationship and we shall address this point in the Discussion.

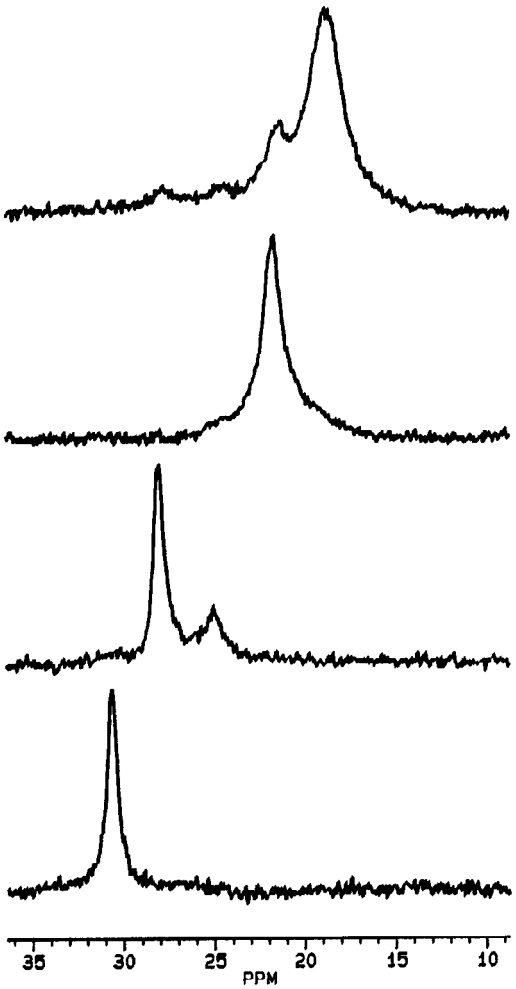

Figure 12. The 36.1 MHz ^{14}N NMR spectra of (from bottom to top) **1-Ar**, **2-Ar** (containing some **3-Ar**), **4-Ar**, and **5-Ar** (containing some **2-Ar**, **3-Ar**, and **4-Ar**) (CH_3CN, 343 K, unlocked, 10 μs (25°) flip angle, 3000 to 5000 scans without recycle delay, acquisition time 0.205 s/scan).

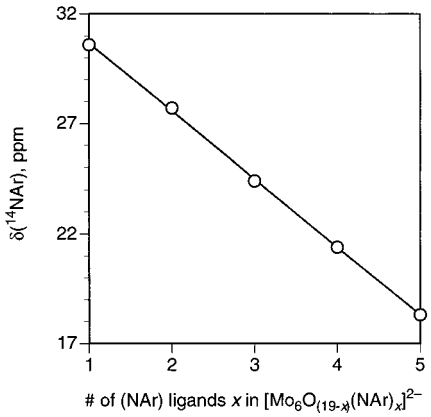

Figure 13. Correlation of $\delta(^{14}NAr)$ with the number of (NAr) substituents in $[Mo_6O_{(19-x)}(NAr)_x]^{2-}$ complexes.

^{17}O NMR Spectroscopy. ^{17}O NMR spectra were recorded in natural abundance for the complexes and a summary is presented in Table 7. For each complex studied, the number and relative intensities of the observed terminal (O_t) and bridging (O_b) resonances agree with expectations from symmetry considerations. Thus, the monosubstituted complexes **1-Bu** and **1-Ar** each display two O_t resonances in a 4:1 ratio (**1-Bu**: 916,

(27) Bradley, D. C.; Hodge, S. R.; Runnacles, J. D.; Hughes, M.; Mason, J.; Richards, R. L. *J. Chem. Soc., Dalton Trans.* **1992**, 1663.

Table 7. ^{17}O NMR Data for $[Mo_6O_{(19-x)}(NR)_x]^{2-}$ Complexes[a,b]

complex	$\delta(^{17}O_t)$[c]	$\delta(^{17}O_t)_{wt}$[d]	$\delta(^{17}O_b)$[e]	$\delta(^{17}O_b)_{wt}$[f]
$[Mo_6O_{19}]^{2-}$	933	933	563	563
$[Mo_6O_{18}(NBu)]^{2-}$ (**1-Bu**)	916, 909 (4:1)	915	575, 565, 549 (4:4:4)	563
$[Mo_6O_{18}(NAr)]^{2-}$ (**1-Ar**)	918, 910 (4:1)	916	582, 566, 550 (4:4:4)	566
$[Mo_6O_{17}(NAr)_2]^{2-}$ (**2-Ar**)	900, 892 (2:2)	896	606, 581, 568, 550, 539 (1:4:2:4:1)	567
$[Mo_6O_{15}(NAr)_4]^{2-}$ (**4-Ar**)	862	862	605, 591, 571, 560, 543 (1:4:2:4:1)	574
$[Mo_6O_{14}(NAr)_5]^{2-}$ (**5-Ar**)	848	848	583, 569, 543 (4:4:4)	565

[a] $[Bu_4N]^+$ salts, CH_3CN solution, 343 K. [b] ^{17}O chemical shifts (in ppm) referenced to external H_2O. [c] $O_t = (^{17}O{\equiv}Mo)$ sites. [d] $\delta(^{17}O_t)_{wt} = \sum(n\delta(^{17}O))/\sum(n)$. [e] $O_b = (Mo{-}^{17}O{-}Mo)$ sites. [f] $\delta(^{17}O_b)_{wt} = (1/12)\sum(n\delta(^{17}O))$.

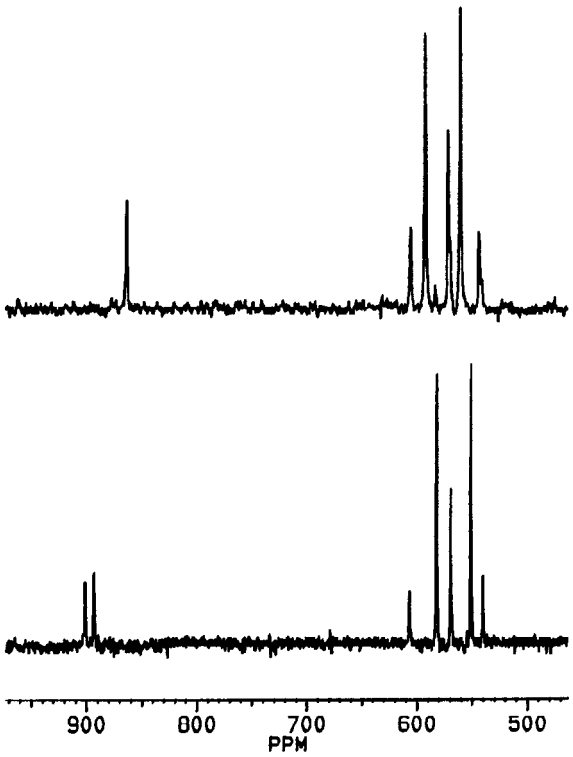

Figure 14. The 67.8 MHz ^{17}O NMR spectra of **2-Ar** (bottom) and **4-Ar** (top) in the O_t and O_b regions (CH_3CN, 343 K, 20 μs (90°) flip angle, 10^6 scans for **2-Ar**, 1.8×10^6 scans for **4-Ar**, without recycle delay, acquisition time 0.025 s/scan).

909 ppm; **1-Ar**: 918, 910 ppm); in each spectrum, the lesser intensity of the upfield signal permits its assignment as the unique O_t site trans to the organoimido ligand.

Figure 14 shows the $^{17}O_t$ and $^{17}O_b$ regions of the spectra of **2-Ar** and **4-Ar**. At the terminal ($^{17}O{\equiv}Mo$) sites of the $[Mo_6O_{(19-x)}(NAr)_x]^{2-}$ systems, a steady upfield progression of $\delta(^{17}O_t)$ accompanies increasing [NAr] incorporation. In fact, as shown in Figure 15, when the weighted average of $\delta(^{17}O_t)$ is plotted vs the number of [NAr] ligands present, a linear correlation is observed. Since $\delta(^{17}O)$ is a sensitive measure of the degree of π-bonding by oxo ligands within congruent sets of complexes,[28] these data clearly indicate that a systematic reduction in bond order at O_t sites accompanies increasing [NAr] incorporation, inferring a buildup of electron density at terminal oxo ligands.

For the bridging ($Mo{-}O{-}Mo$) sites, the weighted averages

(28) (a) Kidd, R. G. *Can. J. Chem.* **1967**, *45*, 605. (b) Filowitz, M.; Klemperer, W. G.; Messerle, L.; Shum, W. *J. Am. Chem. Soc.* **1976**, *98*, 2345. (c) Klemperer, W. G. *Angew. Chem., Int. Ed. Engl.* **1978**, *17*, 246. (d) Klemperer, W. G.; Shum, W. *J. Am. Chem. Soc.* **1978**, *100*, 4892. (e) Filowitz, M.; Ho, R. K. C.; Klemperer, W. G.; Shum, W. *Inorg. Chem.* **1979**, *18*, 93. (f) Miller, K. F.; Wentworth, R. A. D. *Inorg. Chem.* **1979**, *18*, 984. (g) Heath, E.; Howarth, O. W. *J. Chem. Soc., Dalton Trans.* **1981**, 1105. (h) Freeman, M. A.; Schultz, F. A.; Reilley, C. N. *Inorg. Chem.* **1982**, *21*, 567.

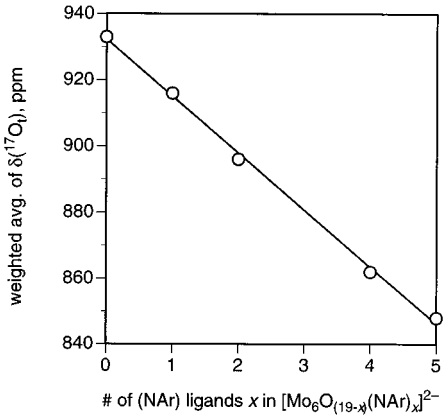

Figure 15. Correlation of $\delta(^{17}O_t)_{wt}$ with the number of (NAr) substituents in $[Mo_6O_{(19-x)}(NAr)_x]^{2-}$ complexes.

of $\delta(^{17}O_b)$ throughout the $[Mo_6O_{(19-x)}(NAr)_x]^{2-}$ series are nearly identical (**1-Ar**, 566 ppm; **2-Ar**, 567 ppm; **4-Ar**, 574 ppm; **5-Ar**, 565 ppm). Furthermore, these values are quite similar to that of the ($^{17}O_b$) resonance in $[Mo_6O_{19}]^{2-}$ (563 ppm), suggesting that the total electronic density at the twelve O_b sites remains essentially invariant throughout the entire series.

Discussion

There are several notable aspects regarding the syntheses of these organoimido hexamolybdates. Unlike previous "assembly" routes to hexamolybdate derivatives, the metathetical approach employed here provides a direct means of functionalization which employs $[Mo_6O_{19}]^{2-}$ as the starting material. These syntheses are broadly systematic and are applicable to a wide variety of organoimido ligand substituents, thus allowing the introduction of a range of appended functionalities. The capability for polyfunctionalization is also noteworthy: the homologous series $[Mo_6O_{(19-x)}(NAr)_x]^{2-}$ described herein provides an opportunity to examine in detail what perturbations arise within the polyoxometalate framework as a result of oxo/imido substitution.

Let us first consider the mono-substituted complexes $[Mo_6O_{18}(NR)]^{2-}$. The cyclic voltammetry results (Table 4) indicate that each of these organoimido derivatives is more electron-rich than is $[Mo_6O_{19}]^{2-}$ with a relative ordering of **1-Cy** $\approx$ **1-Bu** > **1-Ar** > **1-Ph**. The ^{95}Mo NMR spectra (Table 5) of this series reveal a sizable dispersion for the [$^{95}Mo{\equiv}NR$] resonances. Were these [$^{95}Mo{\equiv}NR$] chemical shifts determined *solely* by a dominant diamagnetic shielding term σ_{dia}, then one should expect the shieldings to increase in parallel with the accumulating electron density in the order **1-Ph** < **1-Ar** < **1-Bu** $\approx$ **1-Cy**. In fact, the [$^{95}Mo{\equiv}NR$] resonances for the two most electron-rich systems are observed at highest field in accord with this premise (**1-Cy**: $\delta = 1$; **1-Bu**: $\delta = -2$), but the observed ordering of the two arylimido derivatives (**1-Ph**: $\delta = 68$; **1-Ar**: $\delta = 123$) is contrary to such expectations. A

comparison of the electronic spectra for this group (Table 3) suggests that variations in the paramagnetic shielding term σ_{para} provide a possible explanation for this "anomaly". Note that the visible region λ_{max} values for **1-Cy** (325 nm) and **1-Bu** (329 nm) are similar to that of $[Mo_6O_{19}]^{2-}$ (325 nm), while those of the arylimido systems are red-shifted substantially (**1-Ph**: 342 nm; **1-Tol**: 348 nm; **1-Ar**: 351 nm). Within a congruent set of complexes, the magnitude of the σ_{para} contribution increases as the relevant electron excitation energies decrease. Since enhanced σ_{para} contributions act to deshield a nucleus, driving its chemical shift downfield, it seems likely that the deshielding of **1-Ar** compared to **1-Ph** results from an increased σ_{para} contribution in the former which effectively overrides its relatively larger σ_{dia} component.

The chemical shifts for the [^{95}Mo≡O] sites within the $[Mo_6O_{18}(NR)]^{2-}$ complexes (δ range = 148−153 ppm) are uniformly deshielded compared to those of the [^{95}Mo≡NR] sites within the same complex and also with respect to that of $[Mo_6O_{19}]^{2-}$ (127 ppm). The fact that δ(^{95}Mo≡NR) lies upfield of δ(^{95}Mo≡O) is consistent with the superior electron-donation abilities of organoimido ligands being expressed by larger σ_{dia} contributions. In contrast to the wide variance in the corresponding [^{95}Mo≡NR] resonances, the [^{95}Mo≡O] resonances for **1-Cy**, **1-Bu**, **1-Ph**, and **1-Ar** fall within a narrow range and are insensitive to the system's λ_{max} value. This suggests that variations in σ_{para} are less important in determining these shieldings, and that the downfield chemical shifts are attributable to a decrease in σ_{dia} at these sites. One mechanism by which σ_{dia} could be reduced at the [^{95}Mo≡O] sites is through a diminution of π-donation from the terminal oxo ligands. Our ^{17}O NMR data (Table 7) are consistent with this picture: the $^{17}O_t$ resonances for **1-Bu** and **1-Ar** are shifted upfield of that of $[Mo_6O_{19}]^{2-}$ by ca. 17 ppm, indicative of lessened oxygen-to-molybdenum π-bonding.

Now let us focus on the series of polysubstituted arylimido systems $[Mo_6O_{(19-x)}(NAr)_x]^{2-}$. Each successive incorporation of an [NAr] ligand renders the complex more electron-rich, driving the cluster's $E_{1/2}$ value more negative by ca. 220 mV (Table 4 and Figure 10). Given the steady accumulation of electron density throughout the series, one might expect enhanced σ_{dia} effects to cause a progressive upfield shift of the ^{95}Mo NMR resonances as the degree of substitution increases, yet exactly the opposite trend is observed: as seen in Table 5, the resonances for both the [^{95}Mo≡NAr] and the [^{95}Mo≡O] sites become less shielded with increasing imido incorporation. The downfield shift of δ(^{95}Mo) accompanying progressive [NAr] incorporation is significantly more pronounced for the [^{95}Mo≡O] sites than for the [^{95}Mo≡NAr] sites: the addition of each subsequent [NAr] ligand in the series **1-Ar** through **5-Ar** induces a shift in δ(^{95}Mo≡O) of ca. 18 ppm, while causing a corresponding shift in δ(^{95}Mo≡NAr) of only ca. 6 ppm. The downfield shift of the [^{95}Mo≡O] resonances again is explicable in terms of a reduced σ_{dia} component as discussed above, arising from steadily decreasing π-donation from the terminal oxo ligands: as seen in Table 7 and Figure 15, increasing [NAr] incorporation is accompanied by an upfield progression of δ-(^{17}O≡Mo). Expressed in simple valence bond terms, as the number of [NAr] ligands is increased, electron density builds at the terminal oxo ligands, resulting in a greater contribution from the doubly bonded [Mo═O] canonical form, and a lesser contribution from the [Mo≡O] form.

Insight about the downfield progression in δ(^{95}Mo≡NAr) as the number of [NAr] ligands increases is provided by the electronic spectra of the series (Table 3). Progressive substitution is accompanied by a slight but steady bathochromic shift in the λ_{max} value for the complex. As discussed above, it is likely that these electronic transitions are predominately localized at the [Mo≡NAr] sites and therefore the small downfield progression of δ(^{95}Mo≡NAr) is consistent with the expected slight increase in σ_{para} contributions throughout the series. Another possible contribution to the downfield progression of δ(^{95}Mo≡NAr) is suggested by by our ^{14}N NMR data (Table 6 and Figure 13). The [^{14}NAr] chemical shifts move slightly *upfield* in response to progressive [NAr] incorporation, with each addition causing a change in δ(^{14}NAr) of ca. −3 ppm. This small but steady shielding progression in δ(^{14}NAr) could occur as a result of some electron density "leaking" back out onto the imido nitrogen atoms from the cluster framework, thus diminishing the electron density at the [^{95}Mo≡NAr] sites, leading to a slight but systematic reduction in the σ_{dia} components at Mo. This effect is therefore similar to, but smaller in magnitude than the parallel buildup of electron density observed at the terminal oxo ligands (Figure 15); such a preferential accumulation of electron density at the terminal oxo ligands is in accord with the greater electronegativity of oxygen vs nitrogen. This picture, which postulates that electron density preferentially accumulates at the terminal ligated atoms of the complexes rather than within the $\{Mo_6O_{13}\}$ core, reconciles the overall buildup of electron density with the virtual constancy of the weighted NMR chemical shifts for both the ^{95}Mo atoms (Table 5) and the $^{17}O_b$ atoms (Table 7). Precedence for such an upfield response of organoimido ^{14}N chemical shifts to accumulating electron density is available from a study of a series of methylimido tungsten(VI) complexes of the form *trans*-[MeN≡WCl_4(L)].[29] A steady increase in the ^{14}N shielding of the [NMe] ligand is observed as the electron-donation ability of L increases in the sequence MeCN < $OS(OMe)_2$ < CH_3CO_2Et < $OPMe(OMe)_2$ < $[F]^-$. A similar effect has been observed in the ^{15}N NMR spectra of the d^0 phenylimido complexes [PhN≡$TaCl_3L_2$]: upon changing L from THF to Et_3P, δ(^{15}N) is shifted upfield by 16 ppm.[30]

As a final point, we wish to consider a possible explanation for the observed decrease in reduction potential for the $[Mo_6O_{18}(NR)]^{2-}$ complexes vs that of $[Mo_6O_{19}]^{2-}$ and for the observed cathodic progression in $E_{1/2}$ values for the $[Mo_6O_{(19-x)}(NAr)_x]^{2-}$ complexes with increasing [NAr] incorporation. A detailed theoretical analysis is beyond the scope of this manuscript, and only a simplified presentation will be offered here. $[Mo_6O_{19}]^{2-}$ is a "Type I" polyanion (in Pope's terminology[1a,31]), with each [O≡MoO_5] site displaying virtual tetragonal (C_{4v}) symmetry. Each Mo engages in π-bonding with its terminal oxo ligand producing an *e* (principally O_{2p}) and an *e** (principally d_{xz} and d_{yz}) set of orbitals, assuming each [Mo≡O] vector to lie along a local *z*-axis. In the absence of equatorial Mo−O_b π-bonding (in the *xy* plane), the d_{xy} orbital of each Mo atom is nonbonding and unoccupied. This simple scheme accords with the ready and reversible reductions displayed by $[Mo_6O_{19}]^{2-}$ and other Type I polyoxometalates and is consistent with ESR and optical spectroscopy studies of $[Mo_6O_{19}]^{3-}$.[1a,8b,31−35]

(29) Chambers, O. R.; Harman, M. E.; Rycroft, D. S.; Sharp, D. W. A.; Winfield, J. M. *J. Chem. Res.* **1977**, (*S*) 150, (*M*) 1849.
(30) Rocklage, S. M.; Schrock, R. R. *J. Am. Chem. Soc.* **1982**, *104*, 3077.
(31) Pope, M. T. *Inorg. Chem.* **1972**, *11*, 1973.
(32) Jeannin, Y.; Launay, J. P.; Sanchez, C.; Livage, J.; Fournier, M. *Nouv. J. Chim.* **1980**, *4*, 587.
(33) Sanchez, C.; Livage, J.; Launay, J. P.; Fournier, M.; Jeannin, Y. *J. Am. Chem. Soc.* **1982**, *104*, 3194.
(34) Fournier, M.; Louis, C.; Che, M.; Chaquin, P.; Masure, D. *J. Catal.* **1989**, *119*, 400.
(35) Masure, D.; Chaquin, P.; Louis, C.; Che, M.; Fournier, M. *J. Catal.* **1989**, *119*, 415.

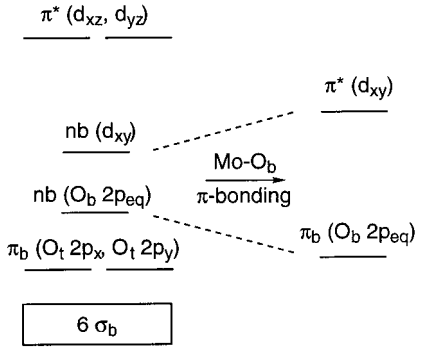

Figure 16. Simplified molecular orbital diagram for the [O≡MoO_5] sites in the $[Mo_6O_{(19-x)}(NR)_x]^{2-}$ systems illustrating the increase in LUMO energy accompanying enhanced Mo−O_b π-bonding.

Note, however, that the Mo d_{xy} orbitals *are* of the proper symmetry to engage in π-bonding with the O $2p_{eq}$ orbitals from the set of four O_b atoms occupying the basal plane at each [Mo≡O] site: such interactions will serve to raise the LUMO energy by producing a π-bonding orbital (principally O_{2p} in character) and a π*-antibonding orbital (principally d_{xy} in character) as shown in Figure 16. The structures of the $[Mo_6O_{18}(NR)]^{2-}$ and $[Mo_6O_{(19-x)}(NAr)_x]^{2-}$ complexes all are indicative of enhanced [Mo−O_b] π-bonding at their [Mo≡O] sites, revealing consistently shorter [Mo−O_b] bonds at the [Mo≡O] sites than at the corresponding [Mo≡NR] or [Mo≡NAr] sites (Figures 4 and 9). At the imido-substituted sites, lengthening of [Mo−O_b] bonds is an expected result of the enhanced electron donation by the organoimido ligands, thus diminishing these Mo atoms' demand for π-bonding from the equatorial set of O_b atoms. Conversely, since our ^{17}O NMR results indicate that a reduction in [Mo≡O] bond order accompanies organoimido incorporation, those Mo atoms bearing terminal oxo ligands should be prone to engage in enhanced π-bonding with their set of four O_b atoms in an attempt to maintain their valence. To the extent that such [Mo−O_b] π-bonding is augmented at the [Mo≡O] sites, the energy of their π^*-d_{xy} LUMOs should be raised, and would therefore be consistent with the trends observed in the cyclic voltammetry data of Table 4 and Figure 10.

Conclusions

Organoimido hexamolybdates constitute a new class of functionalized polyoxometalates, which permit a broad range of appended groups to be incorporated through variations in the imido substituent. This flexibility, coupled with the capacity for polyfunctionalization, has allowed a detailed examination of the perturbations induced by oxo/imido substitution. Each of the organoimido ligands employed here furnishes more electron density to the hexamolybdate cage than does an oxo ligand, rendering the $[Mo_6O_{18}(NR)]^{2-}$ complexes more difficult to reduce than the $[Mo_6O_{19}]^{2-}$ parent; the relative ordering of the systems' $E_{1/2}$ values is in general agreement with the expected inductive effects of the imido substituent. One structural consequence of this enhanced donation is a modest, but consistent, lengthening of the [Mo−O_b] bond lengths at the imido-bearing sites as compared to those at terminal oxo sites.

For the series of polysubstituted arylimido systems $[Mo_6O_{(19-x)}(NAr)_x]^{2-}$, a continual buildup of electron density accompanies increasing arylimido incorporation, as indicated by cyclic voltammetry studies. Multinuclear NMR studies suggest that this electron density accumulates preferentially at the terminal oxo ligands, and to a lesser extent at the imido nitrogen atoms, rather than within the $[Mo_6O_{13}]$ core.

Experimental Section

All syntheses and manipulations were performed under an atmosphere of purified nitrogen, using standard Schlenk, vacuum line, and glovebox techniques. Pyridine and acetonitrile solvents were dried by refluxing in the presence of CaH_2 and were distilled prior to use. $[Bu_4N]_2[Mo_6O_{19}]$ was prepared by a literature method,[8b] and was recrystallized from anhydrous acetonitrile and dried under vacuum before use. BuNCO, CyNCO, and ArNCO were obtained from commercial sources and were used as received. Elemental analyses were performed by Desert Analytics, Tucson, AZ. Cyclic voltammetry studies were performed on CH_3CN solutions at 25 °C in an N_2-filled glovebox using a BAS Model 50 electrochemical workstation employing a Pt working electrode, $[Bu_4N]PF_6$ supporting electrolyte, and a scan rate of 100 mV s^{-1}. $E_{1/2}$ values were measured vs Ag/Ag^+, and $[Bu_4N]_2[Mo_6O_{19}]$ ($E_{1/2} = -707$ mV) was employed as an internal standard; under these conditions, the $[Cp_2Fe]/[Cp_2Fe]^+$ couple was observed at $E_{1/2} = 119$ mV. ^1H NMR spectra were recorded at 400.1 MHz at 298 K using a Bruker WM-400 instrument. ^{17}O, ^{95}Mo, and ^{14}N NMR spectra were recorded at 67.8, 32.6, and 36.1 MHz, respectively, using a Bruker AM 500 spectrometer at 343 K. Some preliminary spectra were obtained at 333 K on a Bruker MSL 400 spectrometer at 54.2 (^{17}O) and 26 MHz (^{95}Mo). All heteronuclear spectra were obtained without lock in anhydrous CH_3CN solutions in 10 mm o.d. NMR tubes. Sample concentrations ranged from about 100 to 150 mg in 2.5 mL of CH_3CN (0.01 to 0.03 M). ^{14}N chemical shifts were measured relative to that of the internal CH_3CN reference and are reported as ppm with respect to neat liquid nitromethane ($\delta(CH_3NO_2) = \delta(CH_3CN) - 135.83$ ppm). ^{95}Mo chemical shifts are reported with respect to that of an external aqueous alkaline solution of 2 M Na_2MoO_4.

$[Bu_4N]_2[Mo_6O_{18}(NBu)]$, 1-Bu. *n*-Butyl isocyanate (0.132 g; 1.3 mmol) was added to a solution of $[Bu_4N]_2[Mo_6O_{19}]$ (1.50 g; 1.1 mmol) in 50 mL of pyridine. After being stirred for 3 d at room temperature, the mixture was filtered, solvent was removed under vacuum, and the residue was washed with Et_2O. The crude product was recrystallized by the slow diffusion of Et_2O vapor into a concentrated CH_3CN solution to produce golden-brown blocks of **1-Bu** (0.9 g; 56%). Anal. Calcd for $C_{36}H_{81}Mo_6N_3O_{18}$: C, 30.46; H, 5.75; N, 2.96. Found: C, 30.56; H, 5.89; N, 2.94. ^1H NMR (CD_3CN, 25 °C): δ 4.59 (t, imido NCH_2, 2 H), 3.10 (m, NCH_2, 16 H), 1.61, (m, imido and cation CH_2, 20 H), 1.36 (m, CH_2, 16 H), 0.96 (m, imido and cation CH_3, 27 H). ^{95}Mo NMR (CH_3CN, 70 °C): δ −2 (t, $^1J_{^{14}N-^{95}Mo} \approx 50$ Hz, *Mo*≡NBu), 152 (*Mo*≡O). ^{17}O NMR (CH_3CN, 70 °C): δ 916, 909 (O_t); 575, 565, 549 (O_b). ^{14}N NMR (CH_3CN, 70 °C): δ 60.9. $\lambda_{max}(\epsilon)$ (CH_3CN, 25 °C): 329 nm (6000). $E_{1/2}$ (CH_3CN): −983 mV.

$[Bu_4N]_2[Mo_6O_{18}(NCy)]$, 1-Cy. Cyclohexyl isocyanate (0.137 g; 1.1 mmol) was added to a solution of $[Bu_4N]_2[Mo_6O_{19}]$ (1.50 g; 1.1 mmol) in 75 mL of pyridine. After being stirred for 3 d at room temperature, the mixture was filtered, solvent was removed under vacuum, and the residue was washed successively with small portions of benzene and Et_2O. The crude product was recrystallized by the slow diffusion of Et_2O vapor into a concentrated CH_3CN solution to produce golden-brown blocks of **1-Cy** (1.17 g; 73%). Anal. Calcd for $C_{38}H_{83}Mo_6N_3O_{18}$: C, 31.57; H, 5.79; N, 2.91. Found: C, 31.73; H, 5.64; N, 2.86. ^1H NMR (CD_3CN, 25 °C): δ 4.55 (m, C*H*, 1 H), 3.12 (m, NCH_2, 16 H), 1.81 (m, Cy CH_2, 10H), 1.62 (m, CH_2, 16 H), 1.38 (m, CH_2, 16 H), 0.97 (t, CH_3, 24 H). ^{95}Mo NMR (CH_3CN, 70 °C): δ 1 (t, $^1J_{^{14}N-^{95}Mo} \approx 50$ Hz, *Mo*≡NCy), 153 (*Mo*≡O). $\lambda_{max}(\epsilon)$ (CH_3CN, 25 °C): 325 nm (7000). $E_{1/2}$ (CH_3CN): −994 mV.

$[Bu_4N]_2[Mo_6O_{18}(NAr)]$, 1-Ar. 2,6-Diisopropylphenyl isocyanate (0.30 g; 1.48 mmol) was added to a solution of $[Bu_4N]_2[Mo_6O_{19}]$ (1.50 g; 1.10 mmol) in 50 mL of pyridine. After being stirred for 3 d at 110 °C, the mixture was filtered, solvent was removed under vacuum, and the residue was washed successively with benzene and with Et_2O. The crude product was recrystallized by the slow diffusion of Et_2O vapor into a concentrated CH_3CN solution to produce red-orange blocks of **1-Ar** (0.83 g; 50%). Anal. Calcd for $C_{44}H_{89}Mo_6N_3O_{18}$: C, 34.68; H, 5.89; N, 2.76. Found: C, 34.73; H, 5.82; N, 2.33. ^1H NMR (CD_3CN, 25 °C): δ 7.17 (d, C_6H_3(*m*), 2 H), 7.06 (t, C_6H_3(*p*), 1H), 3.86 (m, CH(CH_3)$_2$, 2 H), 3.10 (m, NCH_2, 16 H), 1.61 (m, CH_2, 16 H), 1.36 (m, CH_2, 16 H), 1.29 (d, CH(CH_3)$_2$, 12 H), 0.96 (t, CH_3, 24 H). ^{95}Mo NMR

(CH_3CN, 70 °C): δ 123 (t, $^1J_{^{14}N-^{95}Mo} \approx 50$ Hz, *Mo*≡NAr), 152 (*Mo*≡O). ^{17}O NMR (CH_3CN, 70 °C): δ 918, 910 (O_t); 582, 566, 550 (O_b). ^{14}N NMR (CH_3CN, 70 °C): δ 30.6. $\lambda_{max}(\epsilon)$ (CH_3CN, 25 °C): 351 nm (19000). $E_{1/2}$ (CH_3CN): −958 mV.

$[Bu_4N]_2[Mo_6O_{17}(NAr)_2]$, 2-Ar. 2,6-Diisopropylphenyl isocyanate (0.252 g; 1.2 mmol) was added to a solution of $[Bu_4N]_2[Mo_6O_{19}]$ (0.75 g; 0.54 mmol) in 50 mL of pyridine. After being stirred for 8 d at 110 °C, the mixture was filtered, solvent was removed under vacuum, and the residue was washed with Et_2O. The crude product was recrystallized by the slow diffusion of Et_2O vapor into a concentrated CH_3CN solution to produce orange blocks of **2-Ar** (0.61 g; 67%). Anal. Calcd for $C_{56}H_{106}Mo_6N_4O_{17}$: C, 39.96; H, 6.35; N, 3.33. Found: C, 39.59; H, 6.49; N, 3.32. ^1H NMR (CD_3CN, 25 °C): δ 7.14 (d, C_6H_3(*m*), 4 H), 7.02 (m, C_6H_3(*p*), 2H), 3.91 (m, C*H*(CH_3)$_2$, 4 H), 3.11 (m, NCH_2, 16 H), 1.61 (m, CH_2, 16 H), 1.38 (m, CH_2, 16 H), 1.28 (m, CH(CH_3)$_2$, 24 H), 0.95 (t, CH_3, 24 H). ^{95}Mo NMR (CH_3CN, 70 °C): δ 126 (t, $^1J_{^{14}N-^{95}Mo} \approx 50$ Hz, *Mo*≡NAr), 172 (*Mo*≡O). ^{17}O NMR (CH_3CN, 70 °C): δ 900, 892 (O_t); 606, 581, 568, 550,539 (O_b). ^{14}N NMR (CH_3CN, 70 °C): δ 27.7. $\lambda_{max}(\epsilon)$ (CH_3CN, 25 °C): 356 nm (30000). $E_{1/2}$ (CH_3CN): −1168 mV.

$[Bu_4N]_2[Mo_6O_{16}(NAr)_3]$, 3-Ar. 2,6-Diisopropylphenyl isocyanate (3.99 g; 19.6 mmol) was added to a solution of $[Bu_4N]_2[Mo_6O_{19}]$ (1.50 g; 1.1 mmol) in 20 mL of pyridine. After being stirred for 13 d at 110 °C, the mixture was filtered, solvent was removed under vacuum, and the residue was washed twice with small portions of Et_2O. Initial crystallizations (Et_2O/CH_3CN) of the crude product afforded two crops of red crystalline **5-Ar** which were separated by filtration. A small amount of 1,2-dichloroethane (ca. 1 mL) was added to the mother liquor and subsequent slow diffusion of Et_2O vapor afforded dark orange crystals of **3-Ar·3ClCH$_2$CH$_2$Cl** (0.40 g; 17%). Drying under vacuum produced unsolvated **3-Ar**. ^1H NMR (CD_3CN, 25 °C): δ 7.13 (m, C_6H_3(*m*), 6 H), 6.98 (m, C_6H_3(*p*), 3 H), 3.95 (m, C*H*(CH_3)$_2$, 6 H), 3.08 (m, NCH_2, 16 H), 1.60 (m, CH_2, 16 H), 1.35 (m, CH_2, 16 H), 1.29 (m, CH(CH_3)$_2$, 36 H), 0.95 (t, CH_3, 24 H). ^{95}Mo NMR (CH_3CN, 70 °C): δ 130 (*Mo*≡NAr), 191 (*Mo*≡O). ^{14}N NMR (CH_3CN, 70 °C): δ 24.4. $\lambda_{max}(\epsilon)$ (CH_3CN, 25 °C): 361 nm (42000). $E_{1/2}$ (CH_3CN): −1392 mV.

$[Bu_4N]_2[Mo_6O_{15}(NAr)_4]$, 4-Ar. 2,6-Diisopropylphenyl isocyanate (0.464 g; 2.3 mmol) was added to a solution of $[Bu_4N]_2[Mo_6O_{19}]$ (0.75 g; 0.54 mmol) in 30 mL of pyridine. After being stirred for 12 d at 110 °C, the mixture was filtered, solvent was removed under vacuum, and the residue was washed successively with small portions of benzene and Et_2O. Dark orange-red crystals of the solvate **4-Ar·2CH$_3$CN** (0.39 g; 35%) were grown by the slow diffusion of Et_2O vapor into a concentrated acetonitrile/pyridine (9:1) solution. Drying under vacuum produced unsolvated **4-Ar**. Anal. Calcd for $C_{80}H_{140}Mo_6N_6O_{15}$: C, 48.00; H, 7.05; N, 4.20; O, 11.99. Found: C, 47.88; H, 7.02; N, 3.41; O, 11.61. ^1H NMR (CD_3CN, 25 °C): δ 7.10 (m, C_6H_3(*m*), 8 H), 6.95 (m, C_6H_3(*p*), 4 H), 3.99 (m, C*H*(CH_3)$_2$, 8 H), 3.08 (m, NCH_2, 16 H), 1.58 (m, CH_2, 16 H), 1.34 (m, CH_2, 16 H), 1.28 (m, CH(CH_3)$_2$, 48 H), 0.94 (t, CH_3, 24 H). ^{95}Mo NMR (CH_3CN, 70 °C): δ 136 (*Mo*≡NAr), 209 (*Mo*≡O). ^{17}O NMR (CH_3CN, 70 °C): δ 862 (O_t); 605, 591, 571, 560, 543 (O_b). ^{14}N NMR (CH_3CN, 70 °C): δ 21.4. $\lambda_{max}(\epsilon)$ (CH_3CN, 25 °C): 364 nm (58000). $E_{1/2}$ (CH_3CN): −1596 mV.

$[Bu_4N]_2[Mo_6O_{14}(NAr)_5]$, 5-Ar. 2,6-diisopropylphenyl isocyanate (0.967 g; 4.8 mmol) was added to a solution of $[Bu_4N]_2[Mo_6O_{19}]$ (0.75 g; 0.54 mmol) in 20 mL of pyridine. After being stirred for 11 d at 110 °C, the mixture was cooled to room temperature and filtered, solvent was removed under vacuum, and the residue was washed with Et_2O. Drying under vacuum afforded dark red solid **5-Ar** (1.03 g; 86%). Anal. Calcd for $C_{92}H_{157}Mo_6N_7O_{14}$: C, 51.14; H, 7.32; N, 4.54. Found: C, 51.66; H, 7.48; N, 4.61. ^1H NMR (CD_3CN, 25 °C): δ 7.06 (m, C_6H_3(*m*), 10 H), 6.90 (m, C_6H_3(*p*), 5 H), 4.03 (m, C*H*(CH_3)$_2$, 10 H), 3.06 (m, NCH_2, 16 H), 1.57 (m, CH_2, 16 H), 1.33 (m, CH_2, 16 H), 1.28 (m, CH(CH_3)$_2$, 60 H), 0.93 (t, CH_3, 24 H). ^{95}Mo NMR (CH_3CN, 70 °C): δ 146 (*Mo*≡NAr), 225 (*Mo*≡O). ^{17}O NMR (CH_3CN, 70 °C): δ 848 (O_t); 583, 569, 543 (O_b). ^{14}N NMR (CH_3CN, 70 °C): δ 18.3. $\lambda_{max}(\epsilon)$ (CH_3CN, 25 °C): 364 nm (77000). E_{pc} (CH_3CN): −2038 mV (irrev). Dark red crystals of the solvate **5-Ar·2ClCH$_2$CH$_2$Cl** were grown by the slow diffusion of Et_2O vapor into a concentrated CH_3CN solution containing a few drops of 1,2-dichloroethane.

Crystallographic Structural Determinations. Summaries of crystal data, data collection, and refinement parameters are given in Tables 1 and 2. Suitable crystals were selected and mounted in nitrogen-flushed, thin-walled glass capillaries. Unit cell parameters were obtained by the least-squares refinement of the angular settings of 24 reflections ($20° \leq 2\Theta \leq 25°$). No evidence of symmetry higher than triclinic was observed in either the photographic or diffraction data for **1-Cy**, **2-Ar**, and **3-Ar**. The systematic absences in the diffraction data for **1-Bu**, **1-Ar**, and **4-Ar** are uniquely consistent with the reported space groups. The diffraction data for **5-Ar** indicated a *C*-centered monoclinic crystal system. *E*-statistics suggested the centrosymmetric space group options $P(-1)$ for **1-Cy**, **2-Ar**, and **3-Ar** and *C*2/*c* for **5-Ar**. Solution in the assigned space groups yielded chemically reasonable and computationally stable results of refinement. The structures were solved by direct methods, completed by subsequent difference Fourier syntheses and refined by full-matrix least-squares procedures. Semiempirical ellipsoid absorption corrections were applied to **1-Bu**, **2-Ar**, and **4-Ar**, but were not required for **1-Cy**, **1-Ar**, **3-Ar**, and **5-Ar** because there was less than 10% variation in the integrated ψ-scan intensities. The asymmetric units of **1-Cy** and **3-Ar** each contain two independent, but chemically equivalent dianions and four independent, but chemically equivalent cations. One of the cations for **3-Ar** was located only fragmentarily. Three dichloroethane solvent molecules, two acetonitrile solvent molecules, and two dichloroethane solvent molecules were located in the asymmetric units of **3-Ar**, **4-Ar**, and **5-Ar**, respectively. The Mo, N, and O atoms and the *n*-butylimido group's C atoms of **1-Bu**, all non-hydrogen atoms of the dianions of **1-Cy**, all non-hydrogen atoms of **1-Ar**, the Mo, N, and O atoms of **2-Ar**, the Mo atoms of **3-Ar**, all non-hydrogen atoms except one of the two acetonitrile solvent molecules of **4-Ar**, and the Mo, N, and O atoms and the phenyl and tertiary isopropyl carbons of **5-Ar** were refined with anisotropic displacement parameters. All other non-hydrogen atoms were refined isotropically. One of the phenyl rings of **2-Ar** and all of the phenyl rings of **4-Ar** and **5-Ar** were fixed as rigid planar groups. The C−C distances of the isopropyl carbon atoms of **3-Ar** and **5-Ar** were constrained to an average C−C bond length. Due to the high thermal activity of the atoms of one of the solvent molecules of **4-Ar**, the hydrogen atoms on it were omitted. The hydrogen atoms of **3-Ar** were omitted and all other hydrogen atoms were treated as idealized contributions. All software is contained in versions of the SHELXTL 5 libraries of programs (G. Sheldrick, Bruker-AXS, Madison, WI).

Acknowledgment. This work was supported by the United States Department of Energy, Office of Basic Energy Sciences, and by the C.N.R.S.

Supporting Information Available: Tables of crystal data, solution and refinement, atomic coordinates, bond lengths and angles, anisotropic displacement coefficients, and H-atom coordinates for **1-Bu**, **1-Cy**, **1-Ar**, **2-Ar**, **3-Ar**, **4-Ar**, and **5-Ar**; ORTEP diagrams of the second molecules of **1-Cy** and **3-Ar**; ORTEP diagrams of **1-Bu**, **4-Ar**, and **5-Ar** showing atoms as thermal ellipsoids (PDF). X-ray crystallographic files (CIF). This material is available free of charge via the Internet at http://pubs.acs.org.

JA9927974